Chinese Chemical Letters 37 (2026) 111083

Contents lists available at ScienceDirect

Chinese Chemical Letters

journal homepage: www.elsevier.com/locate/cclet

Rational design of a high-efficiency lead halide organic-inorganic hybrid nonlinear optical switch *via* molecular engineering

Xiantan Lin[a,b], Yicong Lv[a,b], Xiaoqi Li[a,c], Zengshan Yue[a], Kai Li[a], Qingyin Wei[a], Qianxi Wang[a], Junhua Luo[a,c,*], Xitao Liu[a,c,*]

[a] State Key Laboratory of Functional Crystals and Devices, Fujian Institute of Research on the Structure of Matter, Chinese Academy of Sciences, Fuzhou 350002, China
[b] College of Chemistry and Materials Science, Fujian Normal University, Fuzhou 350007, China
[c] Fujian College, University of Chinese Academy of Sciences, Fuzhou 350002, China

ARTICLE INFO

Article history:
Received 23 January 2025
Revised 8 March 2025
Accepted 12 March 2025
Available online 31 March 2025

Keywords:
Nonlinear optical switch
Perovskite
Phase transition
Second harmonic generation
High-efficiency

ABSTRACT

As an indispensable subset of functional materials, quadratic nonlinear optical (NLO) switches have garnered increasing attention owing to their vast potential in next-generation intelligent optoelectronic devices. Despite considerable progress in NLO switches based on solid-state phase transitions, identifying an effective strategy to design high-efficiency NLO switches remains a huge challenge. Herein, we present a molecular engineering approach to develop a high-efficiency lead halide organic-inorganic hybrid NLO switch, $(C_8H_{12}N)_2Pb_2Cl_6{\cdot}H_2O$ (NMPTPC). Through the substitution of hydrogen with a methyl group (-CH_3) in protonated N-methylaniline, the initial compound $(C_7H_{10}N)_2Pb_2Cl_6{\cdot}H_2O$ (NMAPC) transformed into NMPTPC retaining the original space group, which gives rise to a dramatic enhancement of second harmonic generation (SHG) and phase transition temperature. As expected, NMPTPC exhibits high-efficiency modulation of the SHG property (2.6 times that of KH_2PO_4) and a high phase transition temperature of 372 K. Notably, NMPTPC exhibits a remarkable temperature-dependent SHG behavior, with an impressive "ON/OFF" ratio of approximately 70, underscoring its significant potential as a high-efficient solid-state NLO switch. Based on in-depth crystal structure analysis and theoretical calculations, the modulation of the NLO property is attributed to the asymmetric distortion of the $[PbCl_6]^{4-}$ octahedra coupled with π-conjugated aromatic amines with a large dipole moment. This research highlights a promising strategy for advancing the development of high-efficiency NLO switches and provides insights into their applications in next-generation intelligent optoelectronic devices.

© 2026 Published by Elsevier B.V. on behalf of Chinese Chemical Society and Institute of Materia Medica, Chinese Academy of Medical Sciences.

Nonlinear optics (NLO) materials have garnered significant attention due to their versatile applications in laser frequency conversion, optical storage, optical information processing and other fields [1–4]. Among them, NLO switches exhibiting a controllable and switchable second harmonic generation (SHG) response, are particularly notable in the field of NLO materials due to their exceptional modulation potential [5,6]. Over the past several decades, a multitude of advanced approaches have been developed to search for NLO switches, including liquid-phase and solid-phase approaches [7,8]. In contrast to liquid-phase transition, solid-state transition induced by temperature changes in materials is regarded as one of the most effective strategies for realizing high-efficiency NLO switches [9]. In these materials, the NLO response undergoes a significant as the compound transitions from the centrosymmetric phase (SHG-OFF state) to the non-centrosymmetric phase (SHG-ON state). As a result, reversible solid-state NLO switches have been obtained in organic molecules, host-guest inclusion complexes, inorganic salts and organic salts [10–15]. For instance, Sun *et al.* reported that the simple organic salt $(Hdabco^+)(CF_3COO^-)$, functions as an SHG switch with an unprecedented switching capacity [16]. However, most of the reported NLO switch compounds are still limited by their poor switching performance, highlighting the need for the design of novel and highly efficient solid-state NLO switches.

Recently, the emerging organic-inorganic hybrid consisting of alternating inorganic and organic components has attracted significant attention owing to exceptional structural flexibility and compositional diversity [17–22]. On one hand, the inorganic framework incorporating second-order Jahn-Teller (SOJT) cations (such as Pb^{2+}, Bi^{3+}, Sb^{3+}, Te^{4+}) exhibits pronounced structural distortions and deformations [23–26]. This characteristic provides a

* Corresponding authors.
E-mail addresses: jhluo@fjirsm.ac.cn (J. Luo), xtliu@fjirsm.ac.cn (X. Liu).

https://doi.org/10.1016/j.cclet.2025.111083
1001-8417/© 2026 Published by Elsevier B.V. on behalf of Chinese Chemical Society and Institute of Materia Medica, Chinese Academy of Medical Sciences.

versatile platform for constructing non-centrosymmetric structures that possess remarkable properties, including nonlinear optical (NLO) functionality. For example, Kang *et al.* reported Pb_2BO_3Cl, a tailor-made polar lead borate chloride, which demonstrates a robust SHG response [27]. Furthermore, Shui *et al.* introduced Pb^{2+} and acetate ions to synthesize halides $Cs_3Pb_2(CH_3COO)_2X_5$ (X = I, Br) with a strong second-harmonic generation response [28]. On the other hand, the flexible and dynamic organic cations offer a high degree of freedom of motion, acting as the driving force for solid-state phase transitions and NLO switching [29]. Furthermore, the introduction of π-conjugated groups [30–34], such as $(C_3N_3O_3)^{3-}$, $(C_9H_{13}N)^+$ and $(C_5H_6ON)^+$ facilitates the achievement of pronounced NLO performance, particularly when incorporating the aromatic amine component. For example, Wu *et al.* reported a non-centrosymmetric organic-inorganic hybrid antimony halide, $(C_9H_{14}N)SbCl_4$, which contains π-conjugated groups and exhibits strong NLO properties [35]. Similarly, Zhang *et al.* reported an antimony-based nonlinear switch, $(C_6H_{14}N)_2SbCl_5$, with phase transition temperatures of 337/332 K [36]. These findings provide valuable guidance for the design of lead halide organic-inorganic hybrids. Methyl groups contribute to stability and by incorporating them into a framework of SOJT cations and π-conjugated groups, this approach offers a novel strategy for achieving stable and efficient nonlinear optical switching.

Herein, lead halide organic-inorganic hybrid NLO switching material $(C_7H_{10}N)_2Pb_2Cl_6{\cdot}H_2O$ (NMAPC), which exhibits an SHG signal comparable to that of KDP, was synthesized. Subsequently, the material $(C_8H_{12}N)_2Pb_2Cl_6{\cdot}H_2O$ (NMPTPC) was synthesized through molecular engineering [37,38], resulting in a significant enhancement of the SHG signal, approximately 2.6 times that of KDP. Thermal analysis and dielectric measurements reveal a solid-state structural phase transition in NMPTPC around 372 K, as indicated by observed changes in its physical properties. Optical property analysis shows that NMPTPC crystals exhibit continuous "SHG-ON" and "SHG-OFF" states with an "ON/OFF" ratio of about 70, indicating that NMPTPC is an efficient NLO switching material. Based on our current understanding, this lead-based halide material demonstrates a significant NLO response and exhibits NLO switching capabilities well above room temperature. This work advances the field of lead halide organic-inorganic hybrid materials, showcasing their potential as NLO switchable materials operating above room temperature.

The bulk colorless single crystals of NMPTPC (inset of Fig. S1a in Supporting information) and NMAPC (inset of Fig. S2 in Supporting information) were obtained using the temperature-cooling method. The mother liquor for growth consisted of an HCl solution containing stoichiometric amounts of $Pb(CH_3CO_2)_2{\cdot}3H_2O$ and organic amines, *N*-methyl-*p*-toluidine ($C_8H_{11}N$), *N*-methylaniline (C_7H_9N). Subsequently, the solution was transferred to an oven set at 338 K for complete dissolution, followed by a gradual cooling process using a predefined temperature control program to achieve saturation. After several weeks, colorless bulk crystals were obtained. The purity and thermal stability of NMPTPC crystals were confirmed through powder X-ray diffraction and thermogravimetric analysis (Fig. S1 in Supporting information), while the crystal purity of NMAPC was also demonstrated (Fig. S2 in Supporting information).

The NMPTPC and NMAPC crystals were crystallized in the orthorhombic asymmetric space group $P2_12_12$ (No. 18) at room temperature. The crystal structures and refinement data of NMPTPC and NMAPC at room temperature are shown in Fig. 1, as well as in Tables S1 and S2 (Supporting information). From the perspective of crystal structure, both NMPTPC and NMAPC consist of inorganic frameworks containing angle-shared and face-shared $[PbCl_6]^{4-}$ octahedra, π-conjugated organic components and free water located at the edges of inorganic frameworks (Fig. 1). The two compounds are distinguished by the presence of *N*-methylaniline in one and

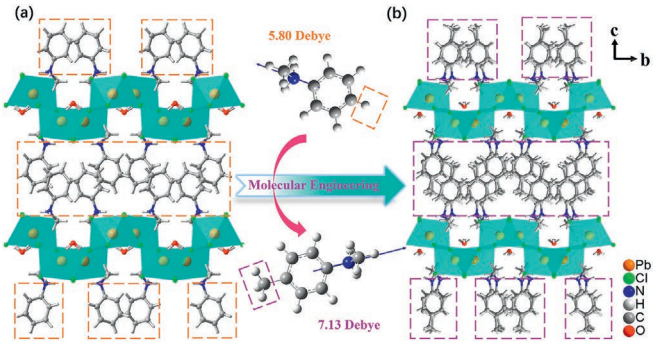


Fig. 1. Molecular engineering perovskite structure. (a) NMAPC structure, (b) NMPTPC structure.

N-methyl-*p*-toluidine in the other organic component. A larger dipole moment can result in several property enhancements, including an increased optical nonlinear response, improved photoelectric conversion efficiency and a stronger SHG response.

The $[PbCl_6]^{4-}$ octahedra of NMPTPC deviates from the ideal structure, exhibiting asymmetric tilt and distortion. The bond length (Pb−Cl) varies from 2.817 Å to 3.166 Å (Table S3 in Supporting information) and the bond angle (Cl−Pb−Cl) varies from 74.84° to 125.86° (Table S4 in Supporting information). The distortion degree of a single octahedron can be measured using the quadratic elongation ($\langle\lambda\rangle$) and the bond angle variance (σ_θ^2), which are defined mathematically as follows [39,40]:

$$\langle\lambda\rangle = \sum_{i=1}^{6} \left(l_i/l_0\right)^2/6 \tag{1}$$

$$\sigma_\theta^2 = \sum_{i=1}^{12} \left(\theta_i - 90^\circ\right)^2/11 \tag{2}$$

where l_i represents the Pb−Cl bond length in a single octahedron, l_0 denotes the average Pb−Cl bond length and θ_i denotes the Cl−Pb−Cl bond angle between neighboring Pb-Cl bonds. The λ value of NMPTPC is calculated as 1.0023, which is higher than that of PEA_2PbI_4 (1.0011), $(BA)_2(MA)Sn_2I_7$ (1.0014) and $(BA)_2(FA)Sn_2I_7$ (1.0020) [40]. In addition, the σ_θ^2 of NMPTPC is 228.4, which is higher than that of $(BA)_2(EA)_2Sn_3Br_{10}$ (30.4) [41]. Such high values of $\langle\lambda\rangle$ and σ_θ^2 generally indicate a significantly distorted octahedron. Furthermore, λ and σ_θ^2 can be used to represent the octahedral distortion. Structural distortion can introduce subtle asymmetries in the lattice, inhibiting the cancellation of the positive and negative frequency components of light, which consequently leads to the generation of a second harmonic [42]. This structural distortion typically induces a reorganization of the electron orbitals, which alters the material's band structure and electron distribution, thereby enhancing or modulating its nonlinear optical response. From the above, the SHG behavior of the NMPTPC crystal largely stems from the distortion of the $[PbCl_6]^{4-}$ octahedron to some degree.

The phase transitions of NMPTPC and NMAPC crystals were characterized by differential scanning calorimetry (DSC) measurements of temperature-dependent permittivity. MNAPC crystals have not received significant attention due to their absence of phase transition (Fig. S3 in Supporting information). The DSC curves show a distinct sharp endothermic peak at 372 K during heating, with a corresponding exothermic peak observed at 337 K during cooling, indicating a reversible phase transition in the NMPTPC crystal (Fig. 2a). The endothermic peak observed during heating and the exothermic peak noted during cooling signify the

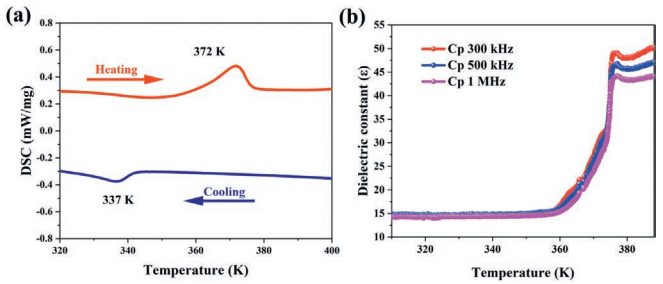


Fig. 2. (a) DSC curves (b) the relationship between the real part of NMPTPC crystal dielectric constant and temperature.

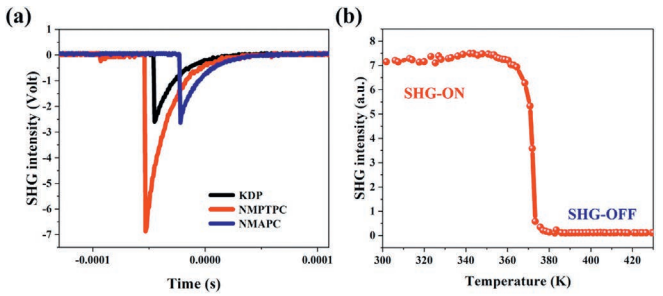


Fig. 3. NLO properties of NMPTPC and NMAPC. (a) SHG intensity. (b) Temperature dependence of SHG signal strength of NMPTPC.

presence of a reversible phase transition dependent on temperature. Molecular dipole motion is often associated with phase transitions and is usually accompanied by significant dielectric anomalies [16,43]. Fig. 2b depicts the real part (ε) of the complex permittivity for an NMPTPC crystal with frequencies of 300 kHz, 500 kHz and 1 MHz as a function of temperature. Notably, the dielectric value of the NMPTPC crystal remains stable and low at temperatures below 372 K. As the temperature surpasses 372 K, the crystal's dielectric value rapidly increases to a high state, consistent with the DSC measurements. Moreover, the complex dielectric constant sustains a high state beyond 372 K. The agreement between the DSC and dielectric constant measurements clearly illustrates the phase transition behavior of NMPTPC.

To assess the applicability of NMPTPC in optical applications, UV–visible diffuse reflectance spectrum was performed on crystalline NMPTPC powders at room temperature. The absorption spectrum of NMPTPC was obtained through the Kubelka–Munk function (Fig. S4 in Supporting information). The optical band gap of NMPTPC is approximately 3.75 eV (inset of Fig. S4). From the absorption spectrum analysis, the absorption cutoff edge of NMPTPC occurs at 320 nm. Analyzing the absorption at the edge of the absorption spectrum suggests that NMPTPC exhibits exceptional transparency beyond 320 nm.

Based on the foregoing analyses, NMPTPC exhibits exceptional properties, including a reversible solid-state phase transition and a non-centrosymmetric structure, both of which are crucial for eliciting the SHG response. Following the approach of Kurtz and Perry [44], with KH_2PO_4 (KDP) as the reference sample, the SHG response of NMPTPC crystal samples was measured under 1064 nm laser irradiation. Comparing the SHG signals of NMPTPC, NMAPC and KDP, NMAPC shows equivalent to KDP, while the SHG signal of NMPTPC is approximately 2.6 times that of KDP (Fig. 3a). The introduction of a larger dipole moment has been proven to be an effective method for enhancing the SHG signal strength. This is primarily because the increase in the dipole moment enhances the

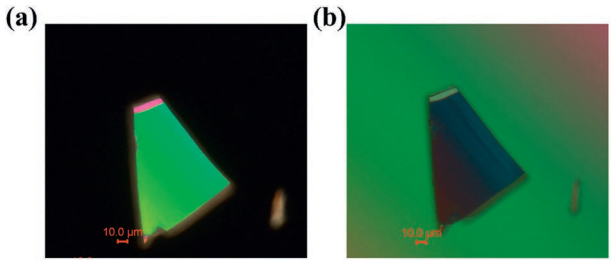


Fig. 4. Birefringence measurement of NMPTPC: (a) The original interference color and (b) the interference color when the crystal is completely extinguished.

material's nonlinear polarization response, significantly amplifying the generation of the second harmonic [45,46]. The organic component is responsible for the difference in SHG response, while the inorganic framework remains unchanged. *N*-Methyl *p*-toluidine has additional methyl groups compared with *N*-methylaniline, which also causes the dipole moments [47] of the two to be different (7.13 Debye for the former and 5.80 Debye for the latter, Fig. 1). Therefore, the NLO signal can be enhanced by modifying their optical properties through molecular engineering [48]. Fig. 3b shows the temperature dependence of the SHG signal for NMPTPC, indicating a heightened SHG response, referred to as the SHG-ON state. The SHG signal rapidly weakens and approaches zero as the temperature increases near 372 K, which is referred to as the SHG-OFF state. As the temperature continues to rise, the SHG signal remains at a low level in the SHG-OFF state (noise error). The switching contrast of NMPTPC is estimated to be around 70, which is significantly higher than that of similar such as $(BA)_2(EA)_2Sn_3Br_{10}$ (35), tellurates α- and β-Li_2HfTeO_6 (13.5), the organic crystal 2-methylpropan-2-aminium 2,2-dimethylpropanoate (19) and the MOF material NH2-MIL-53(Al) (38) [41,49–51]. Additionally, its efficient frequency-doubling switching capability holds great potential for applications in NLO switching.

For ideal NLO materials, moderate birefringence is necessary. Therefore, the NMPTPC crystal (transparent) was selected and cross-polarization microscopy was used to measure and record relevant data for calculating birefringence. The original interference color observed under cross-polarized light was green (Fig. 4a). The extinction of the NMPTPC crystal was achieved by rotating the calibrated quartz wedge compensator (Fig. 4b). The distance rotated through the compensator was compared with the Michal-Levy plot and the delay value (R) was about 1885 nm. Next, the crystal was positioned upright to directly measure the thickness ($d = 17$ μm, Fig. S5 in Supporting information). According to the previously measured values of R and d, the formula $\Delta n = R/d$ was used to calculate the birefringence index of 0.109 at a wavelength of 546 nm, which is comparable to that of some reported inorganic NLO materials such as $Ca_3(BO_3)_2$ (0.097@589 nm) [52], $(C_9H_{14}N)SbCl_4$ (0.095@546 nm) [35] and even exceeds that of others, such as $La(PO_3)_3$ (0.040@1064 nm) and β-$Cd(PO_3)_2$ (0.059@1064 nm) [53]. The moderate birefringence indicates that NMPTPC is an excellent NLO material.

To investigate the underlying reasons for its outstanding optical properties, the density functional theory (DFT) computational method is frequently employed [54]. The band gap value of NMPTPC is calculated to be 3.63 eV (Fig. 5), which is consistent with the experimental results obtained from the UV–vis diffuse reflectance spectra (inset of Fig. S3, band gap = 3.75 eV). The maximum valence band (VBM) and the minimum conduction band (CBM), as shown in the band structure (Fig. 5a), do not appear on the same ordinate, indicating that the compound is an indirect semiconductor. As is well known, electronic transitions near the Fermi energy level govern the optical properties of crystalline ma-

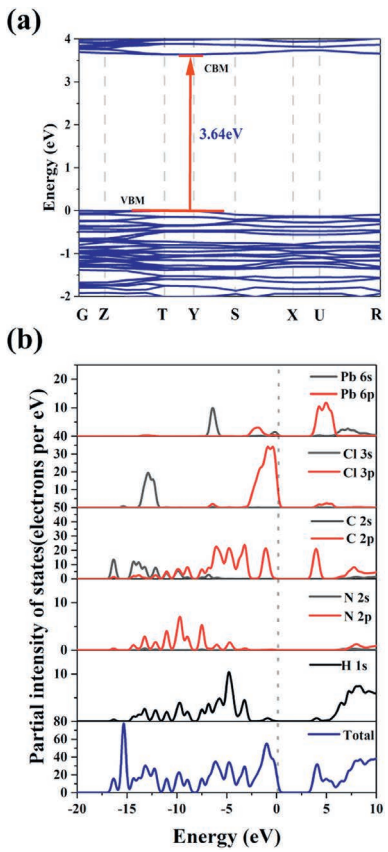


Fig. 5. Electronic characteristics of NMPTPC: (a) Band structure (b) PDOS spectra around the Fermi level.

terials. Therefore, the partial density of states (PDOS) of NMPTPC was analyzed. The covalent interaction between Pb and Cl, forming an octahedron, can be observed through the overlap between Pb and Cl orbitals (Fig. 5b), where the 6s and 6p orbitals of Pb overlap with the 3s 3p orbitals of Cl in the energy range of −20∼10 eV. It can be observed that the C 2p and Cl 3p orbitals primarily appear near the upper limit of the VB, with a small number of N 2p and Pb 6s and 6p orbitals also present nearby. The C 2p, Cl 3p and Pb 6p orbitals are primarily located near the bottom of the CB. At the base of the CB, the orbitals are mainly occupied by the C 2p, Cl 3p and Pb 6p orbitals. The calculation of PDOS and the contribution of each atomic orbital to the density of states provide valuable insights into the optical properties of the crystalline NMPTPC.

Herein, through molecular engineering *via* methyl substitution, we developed a novel lead hybrid perovskite NLO switching material, NMPTPC, with an enhanced NLO response (SHG, 2.6 × KDP) and "ON/OFF" switch ratio of approximately 70. The interaction between Pb^{2+} and the lone pair electrons, combined with the larger dipole moment of the aromatic amine, enhances the SHG signal. These remarkable NLO switching properties render it a promising material for future NLO applications in memory devices and sensors. This work provides a valuable approach for the further exploration of organic-inorganic hybrid metal halides with superior nonlinear optical properties above room temperature.

Declaration of competing interests

The authors declare that they have no known competing financial interests or personal relationships that could have appeared to influence the work reported in this paper.

CRediT authorship contribution statement

Xiantan Lin: Writing – review & editing, Writing – original draft, Investigation, Data curation. **Yicong Lv:** Validation, Supervision, Investigation. **Xiaoqi Li:** Validation, Supervision, Investigation. **Zengshan Yue:** Validation, Supervision, Investigation. **Kai Li:** Validation, Supervision, Investigation. **Qingyin Wei:** Validation, Supervision, Investigation. **Qianxi Wang:** Validation, Supervision, Investigation. **Junhua Luo:** Validation, Supervision, Resources, Project administration, Methodology, Investigation, Funding acquisition. **Xitao Liu:** Validation, Supervision, Resources, Funding acquisition, Conceptualization.

Acknowledgments

This work was supported by the National Natural Science Foundation of China (Nos. 52473283, 22193042, 22125110, 22435005, U21A2069) and the Natural Science Foundation of Fujian Province (No. 2024J010037).

Supplementary materials

Supplementary material associated with this article can be found, in the online version, at doi:10.1016/j.cclet.2025.111083.

References

[1] M. Mutailipu, J. Han, Z. Li, et al., Nat. Photon. 17 (2023) 694–701.
[2] P. Gong, F. Liang, L. Kang, et al., Coord. Chem. Rev. 380 (2019) 83–102.
[3] D. Gounden, N. Nombona, W.E. van Zyl, Coord. Chem. Rev. 420 (2020) 213359.
[4] H. Wu, B. Zhang, H. Yu, et al., Angew. Chem. Int. Ed. 59 (2020) 8922–8926.
[5] M. Samoc, N. Gauthier, M.P. Cifuentes, et al., Angew. Chem. Int. Ed. 45 (2006) 7376–7379.
[6] Z. Sun, T. Chen, X. Liu, et al., J. Am. Chem. Soc. 137 (2015) 15660–15663.
[7] Q. Song, C. Wan, C.K. Johnson, J. Phys. Chem. C 98 (1994) 1999–2001.
[8] K. Nakatani, J.A. Delaire, Chem. Mater. 9 (1997) 2682–2684.
[9] H. Yu, H. Wu, Q. Jing, et al., Chem. Mater. 27 (2015) 4779–4788.
[10] P. Beaujean, F. Bondu, A. Plaquet, et al., J. Am. Chem. Soc. 138 (2016) 5052–5062.
[11] C. Ji, Z. Sun, S. Zhang, et al., Chem. Commun. 51 (2015) 2298–2300.
[12] K. Tao, Z. Wu, S. Han, et al., J. Mater. Chem. C 6 (2018) 4150–4155.
[13] Y. Li, C. Yin, X. Yang, et al., CCS Chem. 3 (2021) 2298–2306.
[14] M.A. Asghar, J. Zhang, S. Han, et al., Chin. Chem. Lett. 29 (2018) 285–288.
[15] H. Sha, D. Yang, Y. Shang, et al., Chin. Chem. Lett. 36 (2025) 109730.
[16] Z. Sun, J. Luo, S. Zhang, et al., Adv. Mater. 25 (2013) 4159–4163.
[17] N. Dehnhardt, M. Axt, J. Zimmermann, et al., Chem. Mater. 32 (2020) 4801–4807.
[18] N. Wang, W. Luo, H. Shen, et al., Chin. Chem. Lett. 35 (2024) 108696.
[19] J. Xu, X. Li, J. Xiong, et al., Adv. Mater. 32 (2020) 1806736.
[20] X. Zhu, L. Zhou, X.Y. Huang, et al., Chin. J. Struct. Chem. 43 (2024) 100272.
[21] D. Fu, L. Pan, Y. Ma, et al., Chin. Chem. Lett. 36 (2025) 109621.
[22] X. Dong, T. Chen, J. Liang, et al., Chin. J. Struct. Chem. 43 (2024) 100256.
[23] K. Kim, M.H. Lee, K.M. Ok, Chem. Mater. 33 (2021) 6564–6571.
[24] M. Yan, H.G. Xue, S.P. Guo, Cryst. Growth Des. 21 (2020) 698–720.
[25] Y. Xu, T. Liu, K. Liu, et al., Nat. Mater. 22 (2023) 1078–1084.
[26] Y. Zhou, L.T. Jiang, X.M. Jiang, et al., Chin. Chem. Lett. 36 (2025) 109740.
[27] K.M. Ok, Chem. Commun. 55 (2019) 12737–12748.
[28] Q.R. Shui, H.X. Tang, R.B. Fu, et al., Angew. Chem. Int. Ed. 60 (2020) 2116–2119.
[29] Y. Li, J. Luo, S. Zhao, Acc. Chem. Res. 55 (2022) 3460–3469.
[30] Y. Kang, Q. Wu, Coord. Chem. Rev. 498 (2024) 215458.
[31] F. Liang, L. Kang, X. Zhang, et al., Cryst. Growth Des. 17 (2017) 4015–4020.
[32] J. Lu, X. Liu, M. Zhao, et al., J. Am. Chem. Soc. 143 (2021) 3647–3654.
[33] Z.P. Zhang, X. Liu, X. Liu, et al., Chem. Mater. 34 (2022) 1976–1984.
[34] P. Gong, X. Liu, L. Kang, et al., Inorg. Chem. Front. 7 (2020) 839–852.
[35] F. Wu, Q. Wei, X. Li, et al., Cryst. Growth Des. 22 (2022) 3875–3881.
[36] J. Zhang, S. Han, X. Liu, et al., Chem. Commun. 54 (2018) 5614–5617.
[37] G. Wu, F. Li, B. Tang, et al., J. Am. Chem. Soc. 144 (2022) 14962–14975.
[38] W. Guo, X. Liu, Z. Sun, Innov. Mater 2 (2024) 100075.
[39] K.Z. Du, Q. Tu, X. Zhang, et al., Inorg. Chem. 56 (2017) 9291–9302.
[40] X. Li, Y. Guan, X. Li, et al., J. Am. Chem. Soc. 144 (2022) 18030–18042.
[41] K. Li, X. Wang, X. Li, et al., Inorg. Chem. 63 (2024) 2275–2281.
[42] K. Lin, P. Gong, S. Chu, et al., J. Am. Chem. Soc. 142 (2020) 7480–7486.
[43] W. Zhang, H.Y. Ye, R. Graf, et al., J. Am. Chem. Soc. 135 (2013) 5230–5233.
[44] S.K. Kurtz, T.T. Perry, J. Appl. Phys. 39 (1968) 3798–3813.
[45] N. Islam, S.S. Chimni, Comput. Theor. Chem. 1086 (2016) 58–66.
[46] Y. Qiu, H. Chen, S. Sun, et al., Chin. Sci. Bull. 52 (2007) 2326–2330.

[47] J. Wudarczyk, G. Papamokos, V. Margaritis, et al., Angew. Chem. Int. Ed. 55 (2016) 3220–3223.
[48] Y. Xie, J. Zheng, K. Zheng, et al., Chem. Mater. 33 (2021) 3081–3086.
[49] D. Wang, Y. Zhang, Q. Shi, et al., Inorg. Chem. Front. 9 (2022) 1708–1713.
[50] Y.L. Luo, L. Zhou, Y.J. Bai, et al., ACS Appl. Mater. Interfaces 16 (2024) 25065–25070.
[51] P. Serra-Crespo, M.A. van der Veen, E. Gobechiya, et al., J. Am. Chem. Soc. 134 (2012) 8314–8317.
[52] S. Zhang, X. Wu, Y. Song, et al., J. Cryst. Growth. 252 (2003) 246–250.
[53] J. Lv, Y. Qian, Q. Jing, et al., Chem. Mater. 34 (2022) 5919–5927.
[54] L. Kang, F. Liang, X. Jiang, et al., Acc. Chem. Res. 53 (2019) 209–217.